European Journal of Pharmaceutical Sciences 192 (2024) 106651

Contents lists available at ScienceDirect

European Journal of Pharmaceutical Sciences

journal homepage: www.elsevier.com/locate/ejps

# *In vitro* biodistribution studies on clinically approved FGFR inhibitors ponatinib, nintedanib, erlotinib and the investigational inhibitor KP2692

Orsolya Dömötör [a,*], Marlene Mathuber [b], Christian R. Kowol [b,c]

[a] Department of Molecular and Analytical Chemistry, University of Szeged, Dóm tér 7-8, 6720 Szeged, Hungary
[b] Institute of Inorganic Chemistry, Faculty of Chemistry, University of Vienna, Waehringer Strasse 42, 1090 Vienna, Austria
[c] Research Cluster "Translational Cancer Therapy Research", University of Vienna and Medical University of Vienna, Vienna, Austria

ARTICLE INFO

*Keywords:*
Blood serum distribution
FGFR
Spectrofluorometry
Protein binding
Binding constant

ABSTRACT

Binding towards human serum albumin (HSA) and α1-acid glycoprotein (AGP) of three approved fibroblast growth factor receptor (FGFR) inhibitors ponatinib (PON), nintedanib (NIN) and erdafitinib (ERD), as well as the experimental drug KP2692 was studied by means of spectrofluorometric and UV–visible spectrophotometric methods. Additionally, proton dissociation processes, lipophilicity, and fluorescence properties of these four molecules were investigated in detail. The FGFR inhibitors were predominantly presented in their single protonated form ($HL^+$) at pH 7.4 (at blood pH). At gastric pH (pH 1–2) the protonated forms (+1 – +3) are present, which provide relatively good aqueous solubility of the drugs. All of the four inhibitors are highly or extremely lipophilic at pH 7.4 ($\log D_{7.4} \geq 2.7$). At acidic pH 2.0 PON and ERD are rather lipophilic, NIN is amphiphilic, while KP2692 is highly hydrophilic. All four compounds bind to HSA and AGP. Moderate binding of PON, KP2692 and NIN was found towards albumin ($\log K' = 4.5–4.7$), while their affinity for AGP was about one order of magnitude higher ($\log K' = 5.2–5.7$). ERD shows a larger affinity for both proteins ($\log K'_{HSA} \approx 5.2$, $\log K'_{AGP} \approx 7.0$). The computed constants were used to model the distribution of the FGFR inhibitors in blood plasma under physiological and pathological (acute phase) conditions. The changing levels of the two proteins under pathological conditions compensate each other for PON and NIN, so that the free drug fractions do not change considerably. In the case of ERD the higher AGP levels distinctly reduce the free available fraction of the drug. Comparison with clinical pharmacokinetic data indicates that the here presented solution distribution studies can very well predict the conditions in cancer patients.

## 1. Introduction

Protein tyrosine kinases phosphorylate various proteins and thus participate in cell growth regulation. Protein tyrosine kinases disorders can cause a series of diseases in the body. Their abnormal expression leads to dysregulation of cell proliferation, which ultimately causes tumorigenesis (Ebrahimi et al., 2023). In addition, these abnormalities are also associated with tumor invasion and metastasis, tumor neovascularization and chemotherapy resistance (Ebrahimi et al., 2023). Therefore, targeting protein tyrosine kinases have become a hot topic in antitumor drug research. After the approval of imatinib (Gleevec®) for the treatment of chronic myeloid leukemia, numerous small molecule tyrosine kinase inhibitors (TKIs) have been introduced into the therapy in the last two decades (Hartmann et al., 2009; Huang et al., 2020). Fibroblast growth factor receptors (FGFR) comprise a main group in the protein tyrosine kinases family, which can be targeted in therapy by non-selective (ponatinib (PON), nintedanib (NIN), lenvatinib, dovitinib *etc.*) and selective (erdafitinib, ERD) FGFR inhibitors (Huang et al., 2020; Lang and Teng, 2019; Perera et al., 2017). These molecules, although being very different in structure, all tend to have poor water solubility and strongly bind to plasma proteins, especially to human serum albumin (HSA) and α1-acid glycoprotein (AGP) (Smith and Waters, 2019; Dömötör et al., 2018; Dosne et al., 2020; Li et al., 2020; Wind et al., 2019; Schmid et al., 2018; Hanley et al., 2022; Gupta et al., 2016). Plasma protein binding influences the pharmacokinetics and efficacy of drugs, because, according to the free drug hypothesis, the unbound fraction of drug is in dynamic equilibrium with respect to metabolism, elimination and interaction with the desired pharmacological target (Summerfield et al., 2022; Rosenbaum, 2017). Albumin prefers to bind negatively charged and neutral small molecules in three main binding

* Corresponding author.
*E-mail address:* domotor.o@chem.u-szeged.hu (O. Dömötör).

https://doi.org/10.1016/j.ejps.2023.106651
Received 4 September 2023; Received in revised form 4 November 2023; Accepted 20 November 2023
Available online 25 November 2023

sites (Sudlow's sites I and II and a third site in subdomain IB), while AGP mostly binds molecules with basic functional group(s) in its central hydrophobic cavity (Smith and Waters, 2019; Peters, 1996; Fanali et al., 2012; Bteich, 2019; Sudlow et al., 1975; Zsila, 2013). A general feature of most of the TKIs is the presence of basic amine group(s) in their structure and the lack of acidic (*e.g.* carboxyl) functions. This raises the possibility of a prominent role for AGP in the transport of these drugs. The physiological concentration of AGP is much lower (approximately 10–20 μM) in blood plasma in comparison to albumin (520–740 μM, 630 μM in average) (Smith and Waters, 2019; Peters, 1996; Fanali et al., 2012) and thus it is more common to observe saturable protein binding when AGP is the main transporter (Smith and Waters, 2019). Additionally, AGP, in contrast to albumin, is a positive acute phase protein, thus its serum concentration increases two- to three-fold during inflammation (Smith and Waters, 2019). It was reported, that increased concentrations of AGP may impact the unbound fraction of drugs in cancer patients, for instance elevated levels of AGP could suppress the cell growth inhibitory effects of paclitaxel and imatinib (Gambacorti--Passerini et al., 2000; Ohbatake et al., 2016). Recently we have assayed the binding affinity of imatinib towards HSA and AGP. It has been demonstrated that AGP plays a more important role in the binding of imatinib compared to HSA and the clinical observations could be supported based on *in vitro* thermodynamic studies (Dömötör and Enyedy, 2023). It has to be mentioned, that also lipoproteins can play an important role in the blood transport of drugs. In particular, the high-, low- and very low-density lipoproteins (HDL, LDL and VLDL) are capable of binding lipophilic substances (Wasan and Cassidy, 1998). However, the here presented work focuses on the elucidation of the relevance of HSA and AGP binding, respectively.

An important question is whether the pharmacokinetic behavior of marketed FGFR inhibitors PON, NIN (formerly referred as intedanib) and ERD (Fig. 1) could be predicted based on simple and cheap *in vitro* binding studies and model calculations. An experimental drug (KP2692), which is a derivative of PON was also included in our studies (Fig. 1). PON is a multi-targeted TKI, it is approved for the treatment of adults with chronic myeloid leukemia or Philadelphia chromosome–-positive acute lymphoblastic leukemia (O'Hare et al., 2009; US Food and Drug Administration, 2012). KP2692 differs from PON in the aliphatic amino functions, an ethylene diamine substituent was introduced instead of the methyl-piperazinyl group making it able to be incorporated in metal complexes (Mathuber et al., 2021). NIN acts as a triple angiokinase inhibitor that inhibits the process of tumor angiogenesis, it is used against idiopathic pulmonary fibrosis and non-small cell lung cancer in combination with docetaxel (European Medicines Agency, 2021; Roth et al., 2015). ERD is a potent oral selective pan-FGFR inhibitor utilized for treatment of metastatic or locally advanced bladder cancer resistant for platinum-based therapy (European Medicines Agency, 2022). The effective dose of ERD has to be individually titrated based on serum phosphate concentration that reflects the extent of FGFR inhibition (Tabernero et al., 2016). It is known from the product monographs that the approved drugs PON, NIN and ERD bind to serum proteins in high extent (>97%). Population pharmacokinetic studies has shown that free fractions of ERD correlate directly with the AGP levels of patients and healthy volunteers (Dosne et al., 2020; Li et al., 2020). Li and coworkers have pointed out that the free fraction of ERD is significantly lower in cancer patients, whose AGP levels are generally elevated, in contrast to the healthy population (0.32% *vs.* 0.51%) (Li et al., 2020). In the case of PON and NIN serum protein binding was tested *in vitro* (*i.e.* the drugs were mixed with freshly taken blood plasma) and preferential binding of NIN towards albumin was found. Further *in vitro* spectroscopic studies are available on the HSA binding of PON, NIN and ERD, however their reliability is sometimes questionable because of the lack of correction by the high absorbance of the samples in fluorometric assays (Amir et al., 2021; Alam et al., 2016) or applying drug concentrations far over their solubility limit (Alam et al., 2016). Only one paper reports on the AGP binding of NIN, however do not account for the absorbance of NIN in fluorometric measurements and most likely misinterpret the results of the UV-visible (UV–vis) binding assay (Abdelhameed et al., 2016). Binding constants on the HSA binding of the marketed TKIs are reported sporadically in the literature and they are often not comparable to each other, while no binding constants on the AGP binding was found for PON and NIN.

Hereby, we report on an extensive comparative study of three approved FGFR inhibitors and KP2692 regarding their proton dissociation processes, lipophilicity and their HSA and AGP binding affinities investigated by means of UV–vis spectrophotometry and spectrofluorometric techniques. Fluorescence properties of the compounds are discussed as well. The obtained binding constants were used to model the serum protein binding of each drugs at physiological and acute phase conditions and compared to those of clinical pharmacokinetic data.

## 2. Materials and methods

### 2.1. Chemicals

All solvents were of analytical grade and used without further purification. KCl, NaCl, HCl, KOH, $NaH_2PO_4$ and $Na_2HPO_4$, warfarin, HSA containing fatty acids (A8763) and AGP (G98885) were purchased from Sigma Aldrich. Ponatinib (PON), nintedanib (NIN) and was purchased from LC Laboratories and erdafitinib (ERD) from ChemScene all in >98% purity. KP2692 was synthesized according to the literature (Mathuber et al., 2021). Doubly distilled Milli-Q water was used for

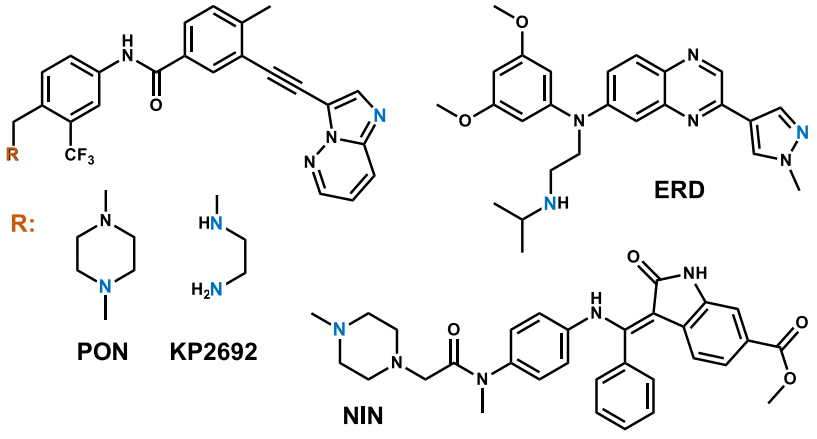


**Fig. 1.** Chemical structures of the FGFR inhibitors ponatinib (PON), KP2692, nintedanib (NIN) and erdafitinib (ERD) investigated in this work. Protonatable atoms are indicated with blue color.

sample preparation. Samples for albumin binding studies were prepared in phosphate buffered saline (PBS) at pH 7.40. Protein stock solutions were prepared in PBS buffer and their concentration was calculated on the basis of their UV–Vis absorption: $\varepsilon_{280\ nm}$(HSA) = 36,850 $M^{-1}$ $cm^{-1}$, $\varepsilon_{280\ nm}$(AGP) = 24,140 $M^{-1}$ $cm^{-1}$ (Beaven et al., 1974; AlAjmi et al., 2020; Zsila and Iwao, 2007).

Slightly acidic stock solutions ($c$ = 0.2–1 mM; pH ~ 3) of the FGFR inhibitors were prepared, except KP2692, that could be dissolved in water ($c$ = 1 mM) and their concentrations were determined based on a weight-in-volume basis. In HSA binding experiments these stocks were diluted with water to get the working solutions ($c$ = 200 μM).

### 2.2. UV–vis spectrophotometric studies: determination of $pK_a$ values

An Agilent Carry 8454 diode array spectrophotometer was used to obtain UV–vis spectra in the interval 190–1100 nm, the path length ($l$) was 0.5, 1.0 or 2.0 cm. The spectrophotometric titrations were performed with samples containing 10–100 μM compound over the pH range 1.0–11.5 at 25.0 ± 0.1 °C and an ionic strength of 0.10 M (KCl). All compounds were titrated twice and at least 20 titration points were collected for each titration. The titrations were performed with carbonate-free KOH solution (0.10 M) and its exact concentration was determined by pH-potentiometric titrations. The electrode system was calibrated to the pH = $-\log[H^+]$ scale by means of blank titrations (strong acid *vs.* strong base; HCl *vs.* KOH), similar to the method suggested by Irving et al. (Irving et al., 1967). Proton dissociation constants together with the individual molar absorbance spectra were calculated with the computer program HypSpec (Gans et al., 1996). The program requires the following input data: measured spectra together with the corresponding pH and analytical (total) concentration of the compounds; species matrix, with approximate protonation constant(s) and the absorbing species need to be defined. Newton-Raphson iterative method is used to obtain protonation constant(s) with standard deviations and molar spectra of the individual species.

### 2.3. Lipophilicity

Distribution coefficients ($D_{pH}$) of the compounds were determined by the traditional shake-flask method in *n*-octanol/buffered aqueous solution generally at pH 2.00 (0.01 M HCl), and pH 7.40 (PBS) at 25.0 ± 0.2 °C as described previously (Enyedy et al., 2011). For NIN $D_{pH}$ was determined at various pH values in order to calculate the p$K_a$ of the drug: pH = 5.60 (20 mM MES buffer, 0.1 M KCl); pH = 6.21, 6.72, 7.19, 7.69 (20 mM phosphate, 0.1 M KCl); pH = 8.13, 8.61, 9.06, 9.62, 10.04 (20 mM borate buffer, 0.1 M KCl). The ligand was dissolved in *n*-octanol pre-saturated aqueous solution of the buffer at 10 μM concentrations. Then the aqueous sample was mixed with *n*-octanol in 1:1, 10:1 or 100:1 vol ratio. Always three parallel measurements were done. After phase separation, UV–vis spectrum of the compound in the aqueous phase was compared to that of the original stock solution and $D_{pH}$ value of the compounds was calculated according to the following equation:

$$D_{pH} = \left[\frac{\text{Abs}_{(stock\ sol.)}}{\text{Abs}_{(aq.\ phase\ after\ separation)}} - 1\right] \times \frac{\text{V}_{(aq.\ phase)}}{\text{V}_{(n-octanol)}}$$

### 2.4. Interaction with serum proteins

#### 2.4.1. Spectrofluorometric measurements

Steady state fluorescence spectra were recorded on a Fluoromax (Horiba, Jobin Yvon) spectrofluorometer. Samples were measured in 1 × 1 cm cells at 37 °C. Titrations were carried out. Samples usually contained (i) 0.5–1 μM protein and various protein-to-compound ratios (up to 1:35) were used, or (ii) the compound concentration was constant (2–6 μM) and the protein concentration varied between 0 and 78 μM. The excitation and emission wavelengths were chosen according to the studied system, see Table S1 for details. The conditional binding constants were calculated with the computer program HypSpec (Gans et al., 1996) as described in our previous works (Dömötör et al., 2013; Enyedy et al., 2015). Calculations were always based on data obtained from at least two independent measurements. 3D spectra were recorded between 250 and 500 nm excitation and 280–650 nm emission wavelengths with an increment of 5 nm. Corrections for self-absorbance and inner filter effect were necessary in the steady-state fluorometric experiments since the emitted light was partly absorbed by the compounds. Corrections for self-absorbance and inner filter effect were done as described in our former works using the formula suggested by Lakowicz (Lakowicz, 2006; Dömötör et al., 2013; Enyedy et al., 2015).

Time-resolved fluorescence measurements on PON and KP2692 were carried out on the same fluorometer equipped with a DeltaHub TCSPC controller using NanoLED light sources N-300 or N-360 (Horiba Jobin Yvon). The resolution of the system was 25 ps. See details on the instrument settings in Table S2. Ludox® (from Sigma-Aldrich) was used as scatter solution to obtain the instrument response function (IRF). On the basis of blank measurements, no background subtraction was necessary. The software DAS6 (version 6.6.; Horiba, Jobin Yvon) was used for the analysis of the experimental fluorescence decays. The fluorescence intensity (*Int.*) decay over time is described by a sum of exponentials,

$$Int.(t) = \sum_{i=1}^{n} \alpha_i exp\left(\frac{-t}{\tau_i}\right) \quad (1)$$

where $\alpha_i$ and $\tau_i$ are the normalized amplitude ($\Sigma\alpha_i = 1$) and lifetime of component $i$ respectively.

From these parameters, the fraction of emitted light ($f$) by each component $i$ can be calculated through the Eq. (2).

$$f_i = \frac{\alpha_i \tau_i}{\sum(\alpha_i \tau_i)} \quad (2)$$

The quality of the fit was judged from a $\chi^2_R$ value close to 1.0 ($\chi^2_R \leq$ 1.20) and a random distribution of weighted residuals. Decay curves always were recorded for three independent samples and standard deviations were calculated for the three measurements.

## 3. Results and discussion

### 3.1. Proton dissociation processes and lipophilicity of the TK inhibitors

The proton dissociation constants (p$K_a$) were determined by UV–vis spectroscopic titrations and in some cases by *n*-octanol/water partition

**Table 1**
Proton dissociation constants (p$K_a$) of the studied inhibitors determined by UV–Vis spectrophotometry[a], calculated distribution (%) of the species in different protonation states at physiological pH (pH 7.40) and the *n*-octanol/water distribution coefficients (log$D_{7.4}$)[b] at pH 7.40 {$T$ = 25 °C; $I$ = 0.1 M (KCl)}.

| | PON | KP2692 | NIN | ERD |
|---|---|---|---|---|
| **p$K_a$($H_3L^{3+}$)** | – | 2.77 ± 0.01 | – | – |
| **p$K_a$($H_2L^{2+}$)** | 2.74 ± 0.01 | 5–7 | – | 1.88 ± 0.01 |
| **p$K_a$($HL^+$)** | 7.8[c] | 8.9 ± 0.1[c] | 8.2 ± 0.1[d]<br>8.1 ± 0.1[e] | 9.10 ± 0.01 |
| | **Protonation states at pH 7.40 (%)** | | | |
| **$H_2L^{2+}$** | 0 | 0.4–28 | 0 | 0 |
| **$HL^+$** | 71 | 70–96 | 82 | 98 |
| **L** | 29 | 2–3 | 18 | 2 |
| ***n*-Octanol/water distriubution** | | | | |
| **log$D_{2.0}$** | +0.59 ± 0.05 | –1.00 ± 0.05 | –0.01 ± 0.02 | +0.24 ± 0.05 |
| **log$D_{7.4}$** | >3.5 | +2.7 ± 0.2 | +3.1 ± 0.2 | +2.7 ± 0.2 |

[a] Standard deviations were calculated based on the titration points of two titrations.
[b] Standard deviations are calculated from three measurements.
[c] Reported in Ref (US Food and Drug Administration, 2012);.
[d] Estimated on the basis of UV–vis titrations.
[e] Calculated from *n*-octanol/water distribution constants determined at various pH values.

experiments and are collected in Table 1. The studied compounds have exclusively basic functional groups, the neutral structures shown in Fig. 1 are the completely deprotonated forms of these substances, having very limited solubility.

Two p$K_a$ values could be determined for ERD; the UV–vis spectra in Fig. 2 show characteristic changes between pH 1–3 and 8–10. The first deprotonation (p$K_a$($H_2L^{2+}$) = 1.88 ± 0.01) can be attributed to the pyrazolium group. The second deprotonation (p$K_a$($HL^+$) = 9.10 ± 0.01) is followed by a less pronounced spectral shift (see Figs. 2 and S1) and occurs due to the deprotonation of the secondary ammonium functional group. Individual molar spectra are plotted in Figure S1. This later constant agrees well with the value (p$K_a$ = 9.2) reported without any reference by Perera et al. (Perera et al., 2017).

PON has one lower p$K_a$ belonging to the heteroaromatic ring system (p$K$($H_2L^{2+}$) = 2.74 ± 0.01), which fits well to the value reported in the product monograph: p$K_a$ = 2.77 (US Food and Drug Administration, 2012). The deprotonation of the piperazinium moiety in PON takes place between pH 7 and 8 (Figure S2(a)). This second p$K_a$ could not be determined by UV–vis titration (Figure S2(b)) and *n*-octanol/water partition due to precipitate formation when the neutral species is formed. According to the product monograph, although no technique and ionic strength were indicated, this value is p$K_a$ = 7.8, which was quoted in Table 1 (US Food and Drug Administration, 2012). This corresponds well to the constant reported for the 1-methyl-piperazinium group in a thiosemicarbazone derivative (p$K_a$ = 7.90, $I$ = 0.1 M KCl) and in cyclizine (p$K_a$ = 8.05) (Bacher et al., 2015; Australian Therapeutic Goods Administration). For KP2692 the lower p$K_a$ of the heteroaromatic ring system (p$K$($H_2L^{2+}$) = 2.77 ± 0.01) is nearly identical to PON. Furthermore, two additional p$K_a$ values were expected for KP2692 based on the analogy of the ethylenediamine moiety to N-methyl-ethylenediamine (p$K_{a1}$ = 7.04, p$K_{a2}$ = 9.98, $I$ = 0.1 M KCl) (Mathuber et al., 2020). One p$K_a$ could be determined in lipophilicity measurements: p$K_a$ = 8.9 ± 0.1 (Table 1, Figure S3). This measurement also indicates a deprotonation step between pH 5–7, which however could not be accurately determined by the available techniques. ChemAxon predicts a p$K_a$ of 6.52. However, the reliability of the prediction has to be questioned if the predicted values for the other compounds are taken into account (Table S3) (MarvinSketch, 2020).

NIN possesses also a methyl-piperazinium group (Fig. 1) and precipitated in titration experiments between pH 7–9 where the neutral species is formed (Figure S4). As Fig. 3 shows, the lipophilicity, namely the *n*-octanol/water distribution coefficient ($D_{pH}$) of NIN rises a few hundred times by the deprotonation of the piperazinium moiety; this phenomenon allowed us to determine a p$K_a$($HL^+$) = 8.1 ± 0.1 for NIN (Table 1), this is in reasonable agreement with the reported (but not referred) value p$K_a$ = 7.9 (Roth et al., 2015).

The knowledge of the relevant proton dissociation constants allowed us to compute fractions for the actual protonation states at pH 7.40

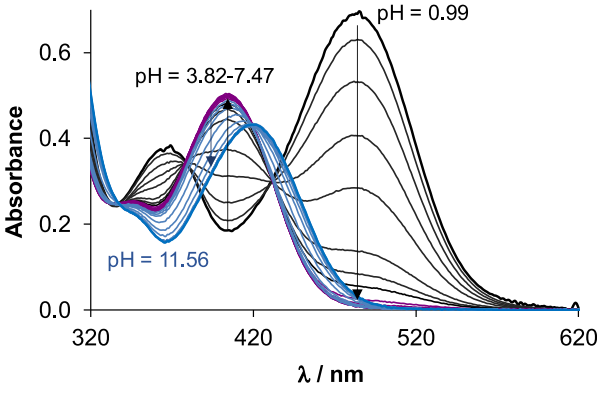


**Fig. 2.** Absorption spectra of ERD recorded in the pH range between 0.99 and 11.56 {$c$ = 40 μM; $I$ = 0.1 M (KCl), $t$ = 25 °C}.

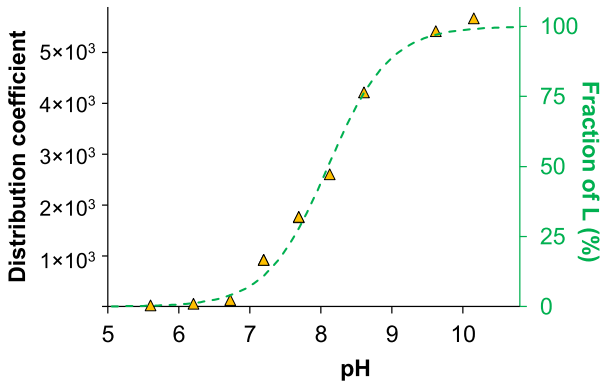


**Fig. 3.** Distribution coefficients (▲) of NIN determined in *n*-octanol/aqueous systems at various pH values plotted together with the calculated molar fraction of the neutral L form (dashed green line) {$I$ = 0.1 M (KCl); $t$ = 25 °C}.

(Table 1) and at various pH values (Figure S5) At pH 7.40, the neural L forms are present in different ratios for PON, NIN and ERD. In the case of PON, this quantity is relatively uncertain, however, using the reported second deprotonation at p$K_a$ = 7.8 (US. Food and Drug Administration, 2012) the neutral form is present in 29%. For NIN and ERD these amounts are 18% and 2%, respectively. KP2692 is mainly protonated and the amount of the neutral form is only between 2 and 3%, however the ratio of $HL^+$ and $H_2L^{2+}$ species are uncertain. At a typically gastric pH of 1–2, all of the studied compounds are present in protonated forms (see Figure S5). The presence of protonated charged species at acidic pH enabled us to prepare stock solutions of the inhibitors of 500 μM at pH 2–3, hence the use of organic solvents (*e.g.* DMSO) could be avoided in the protein binding assays.

The lipophilicity of the studied drugs has been rarely reported in the literature (US Food and Drug Administration, 2012). Table 1 comprises the logarithm of distribution coefficients (log$D_{pH}$) determined at pH 2.0 and 7.4. PON and ERD appear to prefer the non-polar solvent at pH 2.0, NIN distributes approximately equally between the two phases, while KP2692 is rather hydrophilic. At pH 7.4 all of the title compounds are fairly lipophilic (log$D_{7.4}$ ≥ +2.7).

### 3.2. Fluorescence properties of the inhibitors

The knowledge of the fluorescence properties of the three FGFR inhibitors is important as protein binding studies often use fluorescence-based techniques. These data are collected in Table 2. Among the

**Table 2**
Fluorescence characteristics of the studied molecules such as the excitation ($\lambda_{EX}$) and emission ($\lambda_{EM}$) maxima, relative intensities (rel. Int.) determined at the listed wavelengths and at the same slit widths together with the fluorescence lifetime values ($\tau$)[a] obtained at pH 7.4 and 37 °C.

| | | PON | KP2692 | NIN | ERD |
|---|---|---|---|---|---|
| **alone** | $\lambda_{EX}$ (nm) | 305 | 305 | 390 | 385[b] |
| | $\lambda_{EM}$ (nm) | 475 | 475 | 490 | 520 |
| | rel. Int.[c] | 1.00 | 0.64 | 0.004 | 0.008 |
| | $\tau$ (ns) | 4.6 ± 0.1 | 4.7 ± 0.1 | < 0.2 | < 0.2 |
| **with HSA** [c] | $\lambda_{EX}$ (nm) | 305 | 305 | 405 | 385 |
| | $\lambda_{EM}$ (nm) | 455 | 455 | 525 | 475 |
| | $\tau$ (ns) | 10.8 ± 0.1 | 10.9 ± 0.1 | < 0.2 | < 0.2 |
| **with AGP** [c] | $\lambda_{EX}$ (nm) | 305 | 305 | 400 | 385 |
| | $\lambda_{EM}$ (nm) | 440 | 435 | 525 | 517 |
| | $\tau$ (ns) | 11.2 ± 0.2 | 11.4 ± 0.2 | – | – |

[a] Lifetime values and standard deviations are calculated from three independent measurements.
[b] ERD has a second excitation maximum, $\lambda_{EX}$ (nm) = 280 nm, here the emission maximum is the same as in the table.
[c] Calculated at the listed excitation and emission maxima, and normalized for the same concentration. Measured in the presence of 10 equiv. protein.

three molecules, PON and KP2692 display measurable fluorescence emission in aqueous solution as it is shown in Fig. 4 for PON. Similar parameters were reported in ethanol, and cell uptake of PON could be visualized in confocal fluorescence microscopy as well ($\lambda_{EX}$ = 340 nm, $\lambda_{EM}$ = 468 nm) (El Sharkasy et al., 2022; Englinger et al., 2020). Emission spectra were recorded at various pH values and fluorescence lifetime measurement were conducted. Fluorescence lifetime data confirm a single exponential and very similar decay of PON and KP2692 at pH 7.4; $\tau$(PON) = 4.6 ± 0.05 ns, $\tau$(KP2692) = 4.7 ± 0.05 ns (see Figure S6 for the fitted decay curve of PON). NIN and ERD exert nearly negligible fluorescence in acidic aqueous solution and at pH 7.4 (see Figures S7 and S8). The measured intensities are more than two orders of magnitude lower (by using the same slit widths and comparable concentrations) in comparison to PON.

### 3.3. Protein binding studies

The generally poor water solubility of the studied compounds was the main limiting factor for the investigation of the protein binding of PON, KP2692, NIN and ERD. Ultrafiltration was not feasible, because >85% of the TKIs were stuck to the filter. The same problem most likely occurs with the membrane when using equilibrium dialysis. Similarly, the attempt to conduct capillary electrophoresis frontal analysis assays failed due to the lack of sensitivity of the UV–vis detector in the required low micromolar concentration range (1–20 μM). However, spectrofluorometry was able to provide insight in to the protein binding of these molecules via the application of a multitude of techniques. The interaction with AGP and HSA could be followed via protein quenching experiments and the intrinsic fluorescence of the inhibitors, furthermore site marker displacement studies were made as well. Furthermore, UV–vis spectrophotometry was proven to be a useful technique in the case of the NIN – HSA system.

#### 3.3.1. Steady state fluorescence studies via the intrinsic fluorescence of the proteins and the FGFR inhibitors

The 3D fluorescence spectra in Fig. 5 recorded for the HSA – PON system depict the effect of HSA on the fluorescence of PON and *vice versa*. The fluorescence of the protein that originates mainly form the single tryptophan (Trp-214) and several tyrosines (Tyr, 18 moieties) is slightly quenched upon addition of the inhibitor, while PON becomes more fluorescent in the presence of HSA. Similar behavior was found with the other three inhibitors (see Figure S9 for HSA – NIN) and when AGP was used instead of HSA. The emission maxima of the TKIs were shifted to various extents upon binding to the proteins, which are listed in Table 2. The excitation maximum on the other hand, changed only in the case of NIN. The emission peak of PON, KP2692 and ERD showed hypsochromic shift (20–45 nm) when bound to HSA, while NIN displayed a considerable bathochromic shift (35 nm). The AGP binding induced similar changes on spectra of PON, KP2692 and NIN, while only little shifting was observed in the case of ERD (520 nm → 517 nm). Although, blue-shift of emission maxima is often attributed to the binding in hydrophobic cavities of macromolecules, caution is needed here, since little is known about the charge and intermolecular interactions of the bound drugs (Valeur, 2001). The increase of intrinsic fluorescence of the TKIs in all cases suggests that these molecules are bound in pockets protected from water molecules. This phenomenon and the quenching of both proteins allowed to follow the binding interactions from both: the side of the protein and the small molecules. The kinetics of the protein binding was fast (took less than 1 min) in all cases; therefore, titrations were carried out.

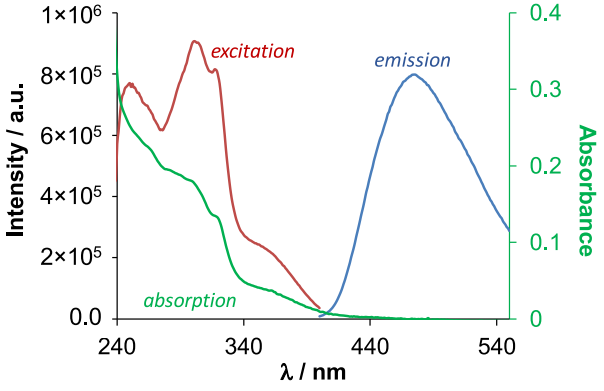


**Fig. 4.** Fluorescence excitation ($\lambda_{EM}$ = 460 nm), emission ($\lambda_{EX}$ = 305 nm) and UV–vis absorption spectra of PON recorded at pH 7.4 in PBS {$c_{PON}$ = 7 μM; $t$ = 37 °C}.

Fig. 6(a) shows a representative example, where the emission band of PON was followed upon addition of AGP. The fluorescence of PON increases and the emission maximum shifts to shorter wavelength (see Table 2). The protein itself has no contribution to the fluorescence of the sample under the applied conditions. Binding constant log$K$' = 5.4 ± 0.1 was calculated with the HypSpec software (Gans et al., 1996) and the fitted titration curve is in good agreement with the experimental data points (Fig. 6(b)). The calculated binding constants for the protein – TKI systems are listed in Table 3. About one order of magnitude lower binding affinity of PON was found with HSA (log$K$' = 4.6 ± 0.1) in comparison to AGP. Protein quenching experiment could not be made with PON, because precipitate formation was observed when its concentration was above 8 μM in the samples. Tayyab et al. reported a very similar quenching constant of $K$' = 4.57 × $10^4$ (log$K$' = 4.66) at 35 °C (Tayyab et al., 2019), although they used no further specified amount of DMSO in the measurements. In the NIN – HSA titration (Fig. 7) the emission intensity of NIN increased dramatically and the protein had only a small contribution to the measured signal. This contribution however was taken into account in the calculations and a log$K$' = 4.5 ± 0.1 could be computed. The bound form is about 50-fold more fluorescent compared to the free NIN. ERD showed somewhat higher binding affinity towards HSA (log$K$' = 5.0 ± 0.1). HSA and AGP quenching experiments were also conducted with NIN and ERD. An example is shown in Fig. 8 for the HSA – ERD system. Table 3 comprises the binding constants obtained by the two methods (intrinsic fluorescence of the TKIs and protein quenching). The calculated quenching constants are somewhat higher for NIN and ERD in comparison to the 'intrinsic' values. There are also literature data reported for the HSA – NIN, HSA – ERD and AGP – NIN systems; quenching constant $K$' = 1.04 × $10^3$, 2.875 × $10^4$ and 1.2 × $10^3$ (log$K$' = 3.02, 4.46, 3.08) were calculated, respectively (Alam et al., 2016; Amir et al., 2021; Abdelhameed et al., 2016). The double logarithmic linearization method, which was applied to obtain binding constant in these papers is a general problem, because it assumes the convergence of the quenching curves to zero intensity, that is often not the case in HSA and AGP quenching experiments (see Fig. 8). This leads to an underestimation of the binding constant, also visible in relation to our constants listed in Table 3. At the same time, the whole picture is further complicated, since correction for self-absorption and inner filter effect was not done, and 2 mM NIN stock solution was prepared in 20 mM phosphate (pH 7.4) for HSA quenching, which is unlikely due to the poor solubility of NIN at this pH value. (Alam et al., 2016; Amir et al., 2021; Abdelhameed et al., 2016). These are most probably the reasons why the reported values strongly differ from here presented results (Table 3).

#### 3.3.2. Site marker displacement studies at site I of HSA

The quenching curve in Fig. 8 for the HSA – ERD system tends to saturation and a log$K$' = 5.3 ± 0.1 could be computed. At the same time, the magnitude of the decrease is not significant, indicating that the binding takes place not necessarily at binding site I. Very similar results were obtained for the HSA – NIN system. Therefore, warfarin displacement experiments were made with ERD, NIN and PON. Warfarin is a well-known site I marker of HSA. It could not displace NIN and ERD from

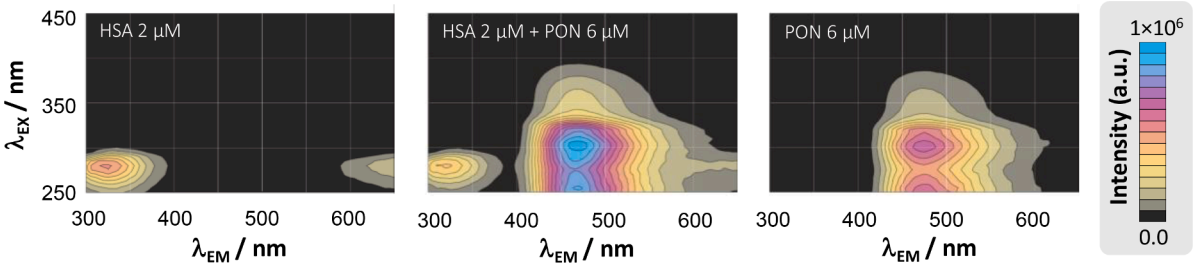


**Fig. 5.** Three-dimensional fluorescence spectra of the HSA – PON system {$c_{HSA}$ = 2.0 μM; $c_{PON}$ = 6 μM; pH = 7.4 (PBS); $t$ = 37 °C}.

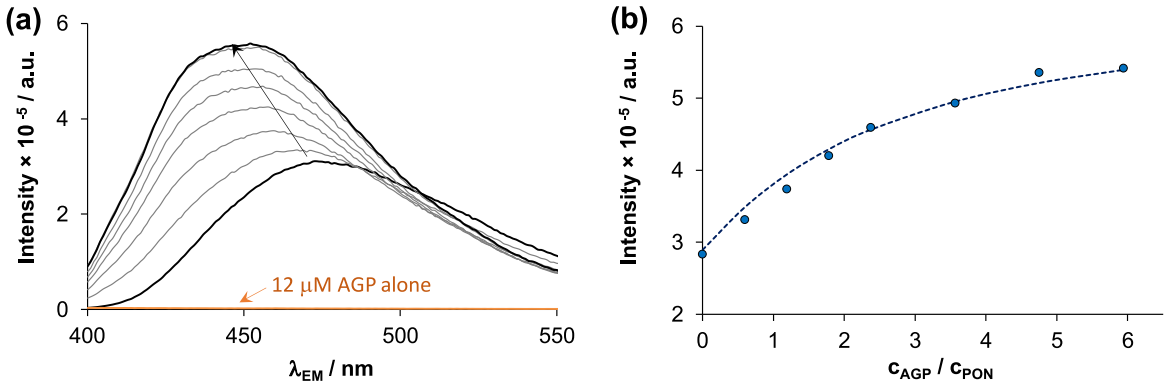


**Fig. 6.** (a) Fluorescence emission spectra obtained by the titration of PON with AGP, the spectrum of AGP (12 μM) is plotted as well for comparison, and (b) the intensity changes at $\lambda_{EM}$ = 460 nm together with the binding curve computed on the basis of the determined binding constant (log$K$' = 5.4 ± 0.1) {$c_{PON}$ = 1.9 μM; $c_{AGP}$ = 0–11 μM; $\lambda_{EX}$ = 310 nm; pH = 7.4 (PBS); $t$ = 37 °C}.

**Table 3**
Conditional binding constants (log$K$')[a] of the compounds on HSA and AGP determined on the basis of protein quenching, intrinsic fluorescence of the drugs and UV–vis titrations, and bound quantities (%) of 1 μM compounds in the presence of the single proteins in physiological concentration {$c_{HSA}$ = 630 μM, $c_{AGP}$ = 15 μM; pH = 7.40 (PBS); 37 °C}.

| | PON | KP2692 | NIN | ERD |
|---|---|---|---|---|
| **HSA** | | | | |
| protein quenching | – | 4.6 ± 0.1 | 4.7 ± 0.1 | 5.3 ± 0.1 |
| intrinsic fluorescence | 4.6 ± 0.1 | 4.5 ± 0.1 | 4.5 ± 0.2 | 5.0 ± 0.1 |
| UV–vis | – | – | 4.6 ± 0.2 | – |
| *bound% ($c_{drug}$ = 1 μM)* | *96* | *96* | *95* | *>99* |
| **AGP** | | | | |
| protein quenching | – | 5.7 ± 0.1 | 5.5 ± 0.1 | 7.1 ± 0.1 |
| intrinsic fluorescence | 5.4 ± 0.1 | 5.5 ± 0.1 | 5.2 ± 0.1 | 6.9 ± 0.1 |
| *bound% ($c_{drug}$ = 1 μM)* | *78* | *85* | *76* | *>99* |

[a] Standard deviations were calculated based on the data points of two titrations.

their binding site and *vice versa* (see Figures S10 and S11). In the case of PON the competition could neither be confirmed nor excluded (Figure S12).

### 3.3.3. *Fluorescence lifetime measurements on the protein binding*

Fluorescence lifetime experiments were carried out for the HSA – PON system. Lifetime experiments may provide information on the number of emitting species with different lifetimes and their quantitative contribution to the measured steady-state fluorescence intensity. PON has a lifetime τ = 4.6 ns (Table 2), however in the presence of HSA (Fig. 9), the decay curves are less steep and two lifetime components could be determined. The first one is identical with the lifetime of free PON, while the second one $\tau_2$ = 10.8 ± 0.1 ns belongs to the protein bound form (see Figure S13). The presence of only one lifetime for the bound form strongly suggest the presence of one single binding site on HSA. While the lifetimes do not depend on the PON-to-HSA ratio, the amplitudes ($\alpha_i$), change in favor of the bound form. Amplitude values are difficult to interpret as direct quantitative indicators, therefore fractional intensities were calculated on the basis of Eq. (2). Fig. 9(b) show the fractional intensities of free and HSA-bound PON in the PON – HSA titration. The end of the titration curve is dominated by the fluorescence of the bound form. Rather similar behavior was obtained for the KP2692 – HSA system. Unfortunately, no lifetime measurements were applicable for the HSA – NIN and HSA – ERD systems as the lifetimes of the protein-bound forms are below the detection limit of the instrument <0.2 ns).

### 3.3.4. *UV–vis spectrophotometric study on the protein binding of NIN*

As Table 2 shows, the excitation maximum of NIN was sensitive to the presence of HSA or AGP, this raises the possibility that the interaction could be followed via the UV–vis absorbance spectra of NIN as well. In Fig. 10 the absorption band of NIN changed tendentiously upon addition of HSA and a bathochromic shift is seen in the absorption maximum. This phenomenon allowed us to calculate an albumin binding constant of 4.6 ± 0.2, which stands in very good agreement with the constants determined in fluorometric experiments. With AGP the spectral changes were not that obvious, consequently no binding constants were calculated. Abdelhameed et al. also intended to follow the interaction of AGP and NIN by UV–vis. However, they followed the absorption band of AGP at 280 nm, where also the added NIN absorbs (see Figure S7) which would require the calculation of difference spectra which was not done (Abdelhameed et al., 2016). The other three TKIs were not suitable for this kind of study, because the absorption band of ERD is not sensitive to the protein binding, while the absorption of PON and KP2692 overlaps with that of the protein band in high extent.

In all, the binding constants listed in Table 3 show, that the four TKIs favor AGP binding over HSA, the calculated binding constants are generally one order of magnitude higher for the AGP – TKI systems. This behavior can be explained easily by structural features. AGP prefers to bind molecules with basic groups, which are present in the studied inhibitors, while albumin prefers more likely neutral or negatively

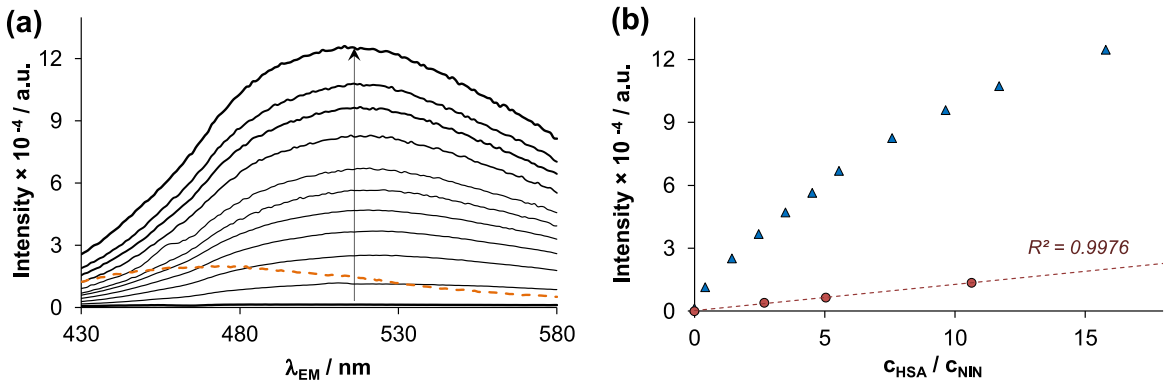


**Fig. 7.** (a) Fluorescence emission spectra obtained by the titration of NIN with HSA, the spectrum of HSA (dashed orange line, 78 μM) is plotted as well for comparison, and (b) the intensity changes at $\lambda_{EM}$ = 500 nm together with the intensities of HSA alone {$c_{NIN}$ = 5.0 μM; $c_{HSA}$ = 0–78 μM; $\lambda_{EX}$ = 390 nm; pH = 7.4 (PBS); $t$ = 37 °C}.

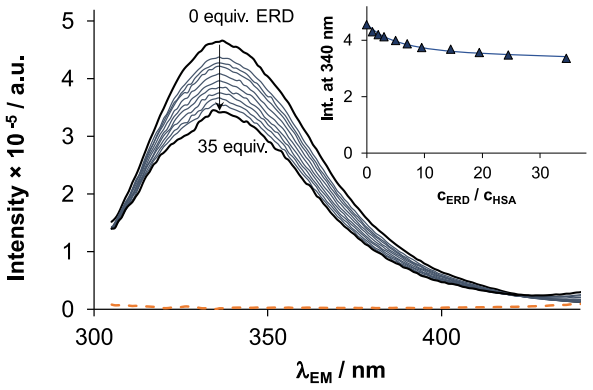


**Fig. 8.** Fluorescence emission spectra of HSA in the absence and presence of ERD, the inserted figure shows the changes of the measured intensity together with the fitted curve (blue line) at $\lambda_{EM}$ = 340 nm. {$c_{HSA}$ = 1.0 μM; $c_{ERD}$ = 0–35 μM; $\lambda_{EX}$ = 295 nm; pH = 7.4 (PBS); $t$ = 37 °C}.

charged small molecules (Peters, 1996; Fanali et al., 2012). Considering the highly lipophilic character of the studied compounds, the binding towards lipoproteins HDL, LDL and VLDL is also possible. The blood concentration of these particles is typically lower than 2 μM. At the same time due to the high hydrophobicity (mainly caused by triglycerides and cholesteryl esters) and large size (7–13 nm diameter) they can accommodate high quantities of drugs. Such binding interactions are well documented among others for cyclosporine A, amphotericin B, and the antidepressants amitriptyline and imipramine (Wasan and Cassidy, 1998). Clinical studies reported on the correlation between hypertriglyceridemia and lower activity of cyclosporine A or decreased nephrotoxicity of amphotericin B. Similarly, the *in vivo* variability in patient's response to the above-listed antidepressants may be at least in part due to varying plasma lipid levels (Wasan and Cassidy, 1998). To the best of our knowledge there are no data about the interaction of PON, NIN or ERD with lipoproteins available. Consequently, to elucidate their impact on the serum protein binding distribution would be of high interest for future studies.

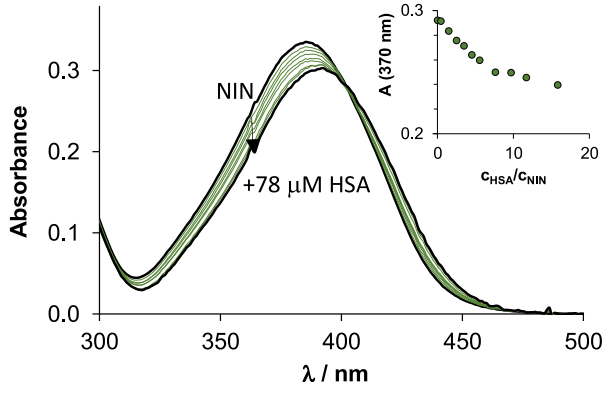


**Fig. 10.** Absorption spectra of NIN in the presence of HSA in various concentrations, the spectra are subtracted by the absorption contribution of HSA; inset: the absorbance changes at 370 nm {$c_{NIN}$ = 5.0 μM; $c_{HSA}$ = 0–78 μM; $\ell$ = 2 cm; pH = 7.4 (PBS); $t$ = 37 °C}.

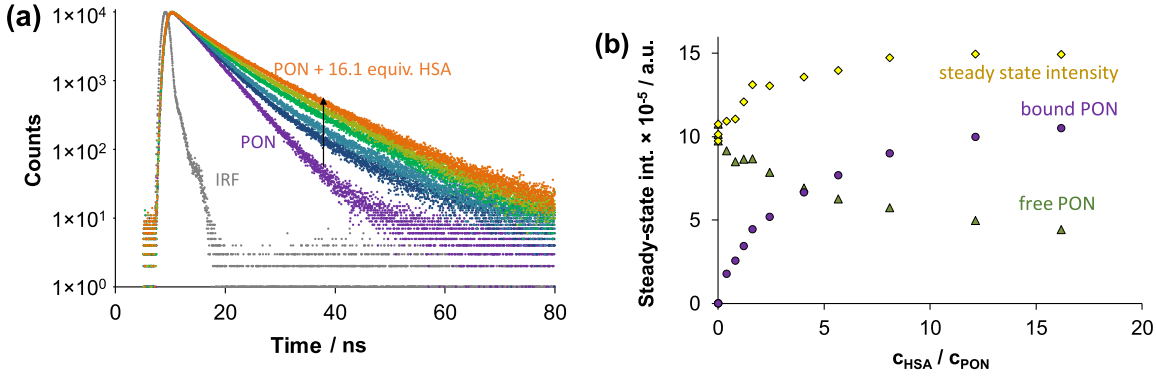


**Fig. 9.** (a) Fluorescence intensity decay of PON in the absence and presence of HSA in various concentrations; IRF: instrument response function recorded for Ludox®; (b) deconvoluted emission intensities of the HSA-bound (●) and free PON (▲) together with the total, steady state intensities (◆) {$c_{PON}$ = 4 μM; $c_{HSA}$ = 0–64 μM; $\lambda_{EX}$ = 300 nm; $\lambda_{EM}$ = 460 nm; pH = 7.4 (PBS); $t$ = 37 °C}.

### 3.4. Model calculations on the blood speciation of the approved drugs

Finally, the different binding preferences at physiological and pathological conditions were investigated through model calculations. Using the bound fractions of the investigated drugs calculated at physiological protein (630 μM HSA or 15 μM AGP) and 1 μM ligand concentration in Table 3 the differences between the TKIs are not significant for the HSA binding (95–>99%). The higher affinity for AGP is compensated for its 24-times lower concentration in blood plasma in contrast to albumin. As expected the highest protein binding is calculated for ERD as for HSA and AGP alone. In order to obtain a more detailed picture on the serum protein binding of these molecules it is necessary to look at ternary systems where (i) the total concentration of the respective drugs corresponds to the clinical values and (ii) the concentration of the two proteins varies within the physiological and pathological levels. Additionally, it is more realistic to show the free concentration of the drugs instead of the bound, because according to the free drug hypothesis the free fraction is responsible for the therapeutic effect (Summerfield et al., 2022; Rosenbaum, 2017). As mentioned in the introduction HSA is a negative acute phase protein, which concentration may decrease in inflammation from 630 μM to as low as 360 μM. AGP on the other side, is a positive acute phase protein, its concentration can increase threefold (45 μM) of the normal level (Smith and Waters, 2019; Peters, 1996; Fanali et al., 2012; Bteich, 2019). The total drug concentrations used for the calculations are average levels found in clinical literature ($c_{PON}$ = 140 nM, $c_{NIN}$ = 60 nM, $c_{ERD}$ = 1500 nM) (Wind et al., 2019; Hanley et al., 2022; Ogura et al., 2015; Dallinger et al., 2016; Scheers et al., 2021; De Zwart et al. 2021).

Fig. 11 shows the calculated free concentrations of each drug. For PON at physiological HSA and AGP concentrations (right front corner in Fig. 11(a)), the free concentration is 4.7 nM. In acute phase reaction the protein concentration changes only slightly to 5.3 nM free PON concentration. Changes in the amount of HSA and AGP compensate each other: the PON released from albumin will be bound by the higher amount of AGP in acute phase conditions (Table S4). Because of the well-comparable binding constants, the same behavior is expected for KP2692. Also the case of NIN is similar, with practically no change in the amount of free drug between physiological ($c_{free}$ = 2.3 nM) and pathological ($c_{free}$ = 2.3 nM) conditions. The two drugs show also dose linearity (see Figure S14), that agrees well with the result of pharmacokinetic studies (Schmid et al., 2018; Hanley et al., 2022). The situation is different for ERD, where the free ligand concentration is distinctly dependent on the amount of AGP, but much less on HSA. Due to a difference of almost two orders of magnitude between the calculated binding constants, ERD binds much stronger to AGP than to HSA. Our calculations show that the concentration of ERD is almost halved ($c_{free}$ = 4.5 nM → 2.3 nM, Fig. 11(c)) at three-fold elevated AGP concentration, which is not compensated by the additional small amount of free drug from lower HSA levels (Table S4). This later model agrees very well with the results of a detailed population pharmacokinetic studies (see Figure S15) (Dosne et al., 2020; Li et al., 2020). Li and coworkers has pointed out that free fraction of ERD is significantly lower in cancer patients, whose AGP levels are generally elevated, in contrast to the healthy population (0.32% *vs*. 0.51%) (Li et al., 2020). The prediction shows *ca.* 0.4% and 0.15% free ERD at physiological (10–15 μM) and pathological (40–45 μM) levels, respectively. The clinical data confirm the reliability of the here presented model calculations, that albumin is not an important factor in the serum protein binding of ERD. Cancer patients with elevated AGP levels may require higher ERD doses as it would be expected from studies assessed on healthy volunteers.

## 4. Conclusions

In this work *in vitro* serum protein binding of three approved FGFR inhibitor anticancer drugs, PON, NIN and ERD as well as the experimental inhibitor KP2692 was investigated by means of spectrofluorometric and UV–vis photometric techniques. In addition to the protein binding assays, proton dissociation processes, lipophilicity at various pH values and fluorescence properties were also studied. All four drugs contain basic amine groups, accordingly the completely deprotonated forms are neutral. The deprotonation constants were determined by UV–vis titrations and *n*-octanol/water distribution experiments between pH 1 and 11.5. At pH 2.0, which corresponds to the gastric pH, they are present as mono-, bi- or trivalent cations which ensures relatively good solubility of these orally administered compounds (≥500 μM). At pH 7.4 (pH of the blood) still the $HL^+$ forms are the major species (70–98%), but the presence of the neutral forms for PON and NIN are also considerable (29% and 18%, respectively). Accordingly, the solubility of the two drugs is reduced to a few micromoles.

The actual protonation states correlate with the lipophilicity. The *n*-octanol/water distribution of the four drugs shows similar tendencies at pH 7.4, all of them are highly-to-extremely lipophilic ($\log D_{7.4} \geq +2.7$). At pH 2.0 PON and ERD are rather lipophilic than hydrophilic, NIN is amphiphilic at this pH while KP2692 is fairly hydrophilic ($\log D_{2.0}$ = –1.00).

PON and KP2692 are fluorescent in aqueous solution, this fluorescence does not depend considerably on the pH of the medium. Fluorescence lifetimes were determined for both compounds in PBS buffer. NIN and ERD display almost negligible fluorescence between pH 2 and 11, and their fluorescence lifetimes were too short (τ≤0.2 ns) for accurate determination.

The literature on the HSA and AGP binding constants of the marketed drugs was rather sparse and data are not very well comparable to each other, additionally no AGP – PON and AGP – NIN binding data were found. The serum protein binding of KP2692 as a new drug candidate was first investigated in this work. Steady-state and time-resolved measurements, as well as fluorescence quenching and site marker displacement experiments were carried out. The binding constants obtained by different techniques are in reasonably good agreement with each other. All the compounds bind to HSA and AGP, but with strong differences in affinities. AGP is favored over the albumin binding in all cases, the calculated binding constants are about one order of magnitude

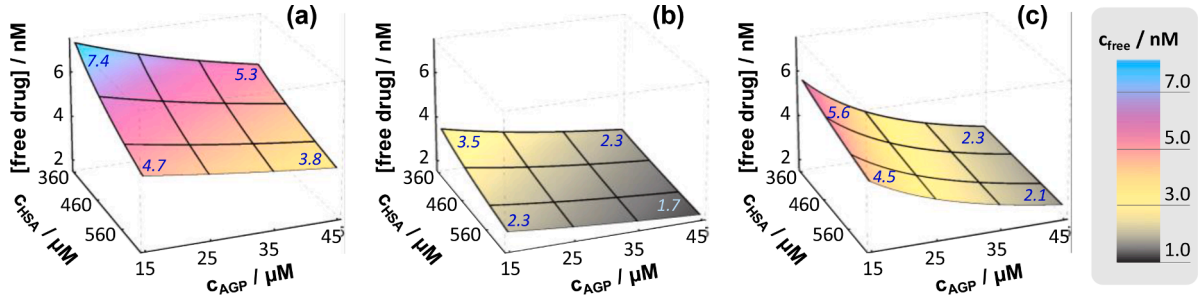


**Fig. 11.** Surface map representation calculated on the free concentration of (a) PON, (b) NIN and (c) ERD by variation of the HSA and AGP levels. The average of binding constants listed in Table 3 were used for the calculations. {$c_{PON}$ = 140 nM; $c_{NIN}$ = 60 nM; $c_{ERD}$ = 1.5 μM}.

higher when the drugs interact with AGP. This phenomenon is most probably due to the observation that AGP prefers the binding of small molecules possessing basic or even positively charged functional groups, while HSA transports more likely molecules of acidic character. ERD showed exceptional high affinity towards AGP (log$K'$ = 6.9–7.1) and also its albumin binding was higher (log$K'$ = 5.0–5.3) in comparison to the other three FGFR inhibitors (log$K'$ = 4.6 in average).

HSA is a negative acute phase protein and hypoalbuminemia is a typical accompanying symptom of chronic inflammation and tumor diseases. Patients with cancer often have increased serum concentrations of the positive acute phase protein AGP. In association with these changes the affinity and the capacity of each plasma protein has to be taken into account both at physiological and pathological conditions when modeling plasma protein binding. Blood distribution of PON, NIN and ERD was modelled under physiological and pathological conditions using the binding data determined in this study. These models showed that for PON and NIN, increased binding to AGP is mostly compensated by the reduced albumin levels and concomitant lower albumin binding. Similar behavior is expected with KP2692 as well. However, in the case of ERD HSA has much less effect on the free drug fraction and AGP levels play a more important role. Our model explains well the clinical observations and the free blood concentration of ERD with half as much in cancer patients as compared to healthy individuals. With the present work, we also aimed to point out that simple and cheap *in vitro* distribution studies can be reliable predictors of the serum protein binding in cancer patients and unveil possible challenges with the pathological serum protein content.

## CRediT authorship contribution statement

**Orsolya Dömötör:** Conceptualization, Data curation, Funding acquisition, Investigation, Writing – original draft. **Marlene Mathuber:** Investigation. **Christian R. Kowol:** Conceptualization, Writing – review & editing.

## Declaration of Competing Interest

The authors declare that they have no known competing financial interests or personal relationships that could have appeared to influence the work reported in this paper.

## Data availability

Data will be made available on request.

## Acknowledgements

O.D. gratefully acknowledges the financial support from a J. Bolyai Research Fellowship (bo-125–20), the ÚNKP-22–5-SZTE-547 – New National Excellence Program and TKP-2021-EGA-32 project of the Development and Innovation Office-NKFIA (Hungary) and University of Szeged Open Access Fund (grant number: 6456).

## Supplementary materials

Supplementary material associated with this article can be found, in the online version, at doi:10.1016/j.ejps.2023.106651.

## References

Abdelhameed, A.S., Ajmal, M.R., Ponnusamy, K., Subbarao, N., Khan, R.H., 2016. Interaction of the recently approved anticancer drug nintedanib with human acute phase reactant α 1-acid glycoprotein. J. Mol. Struct. 1115, 171–179. https://doi.org/10.1016/j.molstruc.2016.02.048.

AlAjmi, M.F., Rehman, M.T., Khan, R.A., Khan, M.A., Muteeb, G., Khan, M.S., Noman, O. M., Alsalme, A., Hussain, A., 2020. Understanding the interaction between α-1-acid glycoprotein (AGP) and potential Cu/Zn metallo-drugs of benzimidazole derived organic motifs: a multi-spectroscopic and molecular docking study. Spectrochim. Acta A Mol. Biomol. Spectrosc. 225, 117457 https://doi.org/10.1016/j.saa.2019.117457.

Alam, P., Abdelhameed, A.S., Rajpoot, R.K., Khan, R.H., 2016. Interplay of multiple interaction forces: binding of tyrosine kinase inhibitor nintedanib with human serum albumin. J. Photochem. Photobiol. B: Biology 157, 70–76. https://doi.org/10.1016/j.jphotobiol.2016.02.009.

Amir, M., Qureshi, M.A., Javed, S., 2021. Biomolecular interactions and binding dynamics of tyrosine kinase inhibitor erdafitinib, with human serum albumin. J. Biomol. Struct. Dyn. 39, 3934–3947. https://doi.org/10.1080/07391102.2020.1772880.

Australian Therapeutic Goods Administration. PM-2010-03573-3-1 Cyclizine lactate https://www.tga.gov.au/resources/auspar/auspar-cyclizine-lactate (accessed 18 July 2023).

Bacher, F., Dömötör, O., Chugunova, A., Nagy, N.V., Filipović, L., Radulović, S., Enyedy, É.A., Arion, V.B., 2015. Strong effect of copper(ii) coordination on antiproliferative activity of thiosemicarbazone–piperazine and thiosemicarbazone–morpholine hybrids. Dalton Trans 44, 9071–9090. https://doi.org/10.1039/C5DT01076D.

Beaven, G.H., Chen, S., D'Albis, A., Gratzer, W.B., 1974. A Spectroscopic study of the haemin-human-serum-albumin system. Eur. J. Biochem. 42, 539–546. https://doi.org/10.1111/j.1432-1033.1974.tb03295.x.

Bteich, M., 2019. An overview of albumin and alpha-1-acid glycoprotein main characteristics: highlighting the roles of amino acids in binding kinetics and molecular interactions. Heliyon 5, e02879. https://doi.org/10.1016/j.heliyon.2019.e02879.

Dallinger, C., Trommeshauser, D., Marzin, K., Liesener, A., Kaiser, R., Stopfer, P., 2016. Pharmacokinetic properties of nintedanib in healthy volunteers and patients with advanced cancer. J. Clin. Pharmacol. 56, 1387–1394. https://doi.org/10.1002/jcph.752.

De Zwart, L., Snoeys, J., Jacobs, F., Li, L.Y., Poggesi, I., Verboven, P., Goris, I., Scheers, E., Wynant, I., Monshouwer, M., Mamidi, R.N.V.S., 2021. Prediction of the drug-drug interaction potential of the α1-acid glycoprotein bound, CYP3A4/CYP2C9 metabolized oncology drug, erdafitinib. CPT Pharmacometric. Syst. Pharmacol. 10, 1107–1118. https://doi.org/10.1002/psp4.12682.

Dömötör, O., Enyedy, É.A., 2023. Evaluation of *in vitro* distribution and plasma protein binding of selected antiviral drugs (favipiravir, molnupiravir and imatinib) against SARS-CoV-2. Int. J. Mol. Sci. 24, 2849. https://doi.org/10.3390/ijms24032849.

Dömötör, O., Hartinger, C.G., Bytzek, A.K., Kiss, T., Keppler, B.K., Enyedy, É.A., 2013. Characterization of the binding sites of the anticancer ruthenium(III) complexes KP1019 and KP1339 on human serum albumin via competition studies. J. Biol. Inorg. Chem. 18, 9–17. https://doi.org/10.1007/s00775-012-0944-6.

Dömötör, O., Pelivan, K., Borics, A., Keppler, B.K., Kowol, C.R., Enyedy, É.A., 2018. Comparative studies on the human serum albumin binding of the clinically approved EGFR inhibitors gefitinib, erlotinib, afatinib, osimertinib and the investigational inhibitor KP2187. J. Pharm. Biomed. Anal. 154, 321–331. https://doi.org/10.1016/j.jpba.2018.03.011.

Dosne, A.G., Valade, E., Stuyckens, K., Li, L.Y., Ouellet, D., Perez-Ruixo, J.J., 2020. Population pharmacokinetics of total and free erdafitinib in adult healthy volunteers and cancer patients: analysis of phase 1 and phase 2 studies. J. Clin. Pharmacol. 60, 515–527. https://doi.org/10.1002/jcph.1547.

Ebrahimi, N., Fardi, E., Ghaderi, H., Palizdar, S., Khorram, R., Vafadar, R., Ghanaatian, M., Rezaei-Tazangi, F., Baziyar, P., Ahmadi, A., Hamblin, M.R., Aref, A. R., 2023. Receptor tyrosine kinase inhibitors in cancer. Cell. Mol. Life. Sci. 80, 104. https://doi.org/10.1007/s00018-023-04729-4.

El Sharkasy, M.E., Aboshabana, R., Belal, F., Walash, M., Tolba, M.M., 2022. Synchronized spectrofluorimetric determination of ponatinib and curcumin as an effective therapeutic combination in laboratory prepared mixtures and human plasma samples. Spectrochim. Acta A 264, 120235. https://doi.org/10.1016/j.saa.2021.120235.

Englinger, B., Laemmerer, A., Moser, P., Kallus, S., Röhrl, C., Pirker, C., Baier, D., Mohr, T., Niederstaetter, L., Meier-Menches, S.M., Gerner, C., Gable1, L., Gojo, J., Timelthaler, G., Senkiv, J., Jäger, W., Kowol, C.R., Heffeter, P., Berger, W., 2020. Lipid droplet-mediated scavenging as novel intrinsic and adaptive resistance factor against the multikinase inhibitor ponatinib. Int. J. Cancer 147, 1680–1693. https://doi.org/10.1002/ijc.32924.

Enyedy, É.A., Hollender, D., Kiss, T., 2011. Lipophilicity of kinetically labile metal complexes through the example of antidiabetic Zn(II) and VO(IV) compounds. J. Pharm. Biomed. Anal. 54, 1073–1081. https://doi.org/10.1016/j.jpba.2010.12.025.

Enyedy, É.A., Dömötör, O., Bali, K., Hetényi, A., Tuccinardi, T., Keppler, B.K., 2015. Interaction of the anticancer gallium(III) complexes of 8-hydroxyquinoline and maltol with human serum proteins. J. Biol. Inorg. Chem. 20, 77–88. https://doi.org/10.1007/s00775-014-1211-9.

European Medicines Agency. 8/11/2021 Vargatef - EMEA/H/C/002569 - IG/1463 https://www.ema.europa.eu/en/medicines/human/EPAR/vargatef (accessed 18 July 2023).

European Medicines Agency. 07/04/2022 Ofev - EMEA/H/C/003821 - II/0046 https://www.ema.europa.eu/en/medicines/human/EPAR/ofev (accessed 18 July 2023).

Fanali, G., di Masi, A., Trezza, V., Marino, M., Fasano, M., Ascenzi, P., 2012. Human serum albumin: from bench to bedside. Mol. Asp. Med. 33, 209–290. https://doi.org/10.1016/j.mam.2011.12.002.

Gambacorti-Passerini, C., Barni, R., Coutre, P., Zucchetti, M., Cabrita, G., Cleris, L., Rossi, F., Gianazza, E., Brueggen, J., Cozens, R., Pioltelli, P., Pogliani, E., Corneo, G., Formelli, F., D'Incalci, M., 2000. Role of alpha1 acid glycoprotein in the *in vivo*

resistance of human BCR-ABL(+) leukemic cells to the abl inhibitor STI571. J. Natl. Canc. Inst. 92, 1641–1650. https://doi.org/10.1093/jnci/92.20.1641.
Gans, P., Sabatini, A., Vacca, A., 1996. Investigation of equilibria in solution. Determination of equilibrium constants with the HYPERQUAD suite of programs. Talanta 43, 1739–1753. https://doi.org/10.1016/0039-9140(96)01958-3.
Gupta, A., Jarzab, B., Capdevila, J., Shumaker, R., Hussein, Z., 2016. Population pharmacokinetic analysis of lenvatinib in healthy subjects and patients with cancer. Br. J. Clin. Pharmacol. 81, 1124–1133. https://doi.org/10.1111/bcp.12907.
Hanley, M.J., Diderichsen, P.M., Narasimhan, N., Srivastava, S., Gupta, N., Venkatakrishnan, K., 2022. Population pharmacokinetics of ponatinib in healthy adult volunteers and patients with hematologic malignancies and model-informed dose selection for pediatric development. J. Clin. Pharmacol. 62, 555–567. https://doi.org/10.1002/jcph.1990.
Hartmann, J.T., Haap, M., Kopp, H.-G., Lipp, H.-P., 2009. Tyrosine kinase inhibitors - a review on pharmacology, metabolism and side effects. Curr. Drug. Metab. 10, 470–481. https://doi.org/10.2174/138920009788897975.
Huang, L., Jiang, S., Shi, Y., 2020. Tyrosine kinase inhibitors for solid tumors in the past 20 years (2001-2020). J. Hematol. Oncol. 13, 143. https://doi.org/10.1186/s13045-020-00977-0.
Irving, H.M., Miles, M.G., Pettit, L.D., 1967. A study of some problems in determining the stoicheiometric proton dissociation constants of complexes by potentiometric titrations using a glass electrode. Anal. Chim. Acta 38, 475–488. https://doi.org/10.1016/S0003-2670(01)80616-4.
Lakowicz, J.R., 2006. Principles of Fluorescence Spectroscopy, third ed. Springer, New York.
Lang, L., Teng, Y., 2019. Fibroblast growth factor receptor 4 targeting in cancer: new insights into mechanisms and therapeutic strategies. Cells 8, 31. https://doi.org/10.3390/cells8010031.
Li, L.Y., Guo, Y., Gonzalez, M., Ouellet, D., 2020. Effect of plasma protein binding on the pharmacokinetics of erdafitinib: results of an integrated cross-study analysis. Pharmacokinet 60 (3), 391–399. https://doi.org/10.1002/jcph.1529.
MarvinSketch. 2020. version 20.9 chemical editor of ChemAxon, https://chemaxon.com/(accessed 18 July 2023).
Mathuber, M., Schueffl, H., Dömötör, O., Karnthaler-Benbakka, C., Enyedy, É.A., Heffeter, P., Keppler, B.K., Kowol, C.R., 2020. Improving the stability of EGFR inhibitor cobalt(III) prodrugs. Inorg. Chem. 17794–17810. https://doi.org/10.1021/acs.inorgchem.0c03083.
Mathuber, M., Gutmann, M., La Franca, M., Vician, P., Laemmerer, A., Moser, P., Keppler, B.K., Berger, W., Kowol, C.R., 2021. Development of a cobalt(III)-based ponatinib prodrug system. Inorg. Chem. Front. 8, 2468–2485. https://doi.org/10.1039/D1QI00211B.
Ogura, T., Taniguchi, H., Azuma, A., Inoue, Y., Kondoh, Y., Hasegawa, Y., Bando, M., Abe, S., Mochizuki, Y., Chida, K., Klüglich, M., Fujimoto, T., Okazaki, K., Tadayasu, Y., Sakamoto, W., Sugiyama, Y., 2015. Safety and pharmacokinetics of nintedanib and pirfenidone in idiopathic pulmonary fibrosis. Eur. Respir. J. 45, 1382–1392. https://doi.org/10.1183/09031936.00198013.
O'Hare, T., Shakespeare, W.C., Zhu, X., Eide, C.A., Rivera, V.M., Wang, F., Adrian, L.T., Zhou, T., Huang, W.-S., Xu, Q., Metcalf III, C.A., Tyner, J.W., Loriaux, M.M., Corbin, A.S., Wardwell, S., Ning, Y., Keats, J.A., Wang, Y., Sundaramoorthi, R., Thomas, M., Zhou, D., Snodgrass, J., Commodore, L., Sawyer, T.K., Dalgarno, D.C., Deininger, M. W.N., Druker, B.J., Clackson, T., 2009. AP24534, a pan-BCR-ABL inhibitor for chronic myeloid leukemia, potently inhibits the T315I mutant and overcomes mutation-based resistance. Cancer Cell 16, 401–412. https://doi.org/10.1016%2Fj.ccr.2009.09.028.
Ohbatake, Y., Fushida, S., Tsukada, T., Kinoshita, J., Oyama, K., Hayashi, H., Miyashita, T., Tajima, H., Takamura, H., Ninomiya, I., Yashiro, M., Hirakawa, K., Ohta, T., 2016. Elevated alpha1-acid glycoprotein in gastric cancer patients inhibits the anticancer effects of paclitaxel, effects restored by co-administration of erythromycin. Clin. Exp. Med. 16, 585–592. https://doi.org/10.1007/s10238-015-0387-9.
Perera, T.P.S., Jovcheva, E., Mevellec, L., Vialard, J., De Lange, D., Verhulst, T., Paulussen, C., Van De Ven, K., King, P., Freyne, E., Rees, D.C., Squires, M., Saxty, G., Page, M., Murray, C.W., Gilissen, R., Ward, G., Thompson, N.T., Newell, D.R., Cheng, N., Xie, L., Yang, J., Platero, S.J., Karkera, J.D., Moy, C., Angibaud, P., Laquerre, S., Lorenzi, M.V., 2017. Discovery and pharmacological characterization of JNJ-42756493 (erdafitinib), a functionally selective small-molecule FGFR family inhibitor. Mol. Cancer. Ther. 16, 1010–1020. https://doi.org/10.1158/1535-7163.MCT-16-0589.
Peters, T., 1996. All About Albumin: Biochemistry, Genetics and Medical Applications. Academic Press, San Diego.
Rosenbaum, S.E., 2017. Basic Pharmacokinetics and Pharmacodynamics, Second ed. Wiley, Hoboken, New Jersey.
Roth, G.J., Binder, R., Colbatzky, F., Dallinger, C., Schlenker-Herceg, R., Hilberg, F., Wollin, S.-L., Kaiser, R., 2015. Nintedanib: from discovery to the clinic. J. Med. Chem. 58, 1053–1063. https://doi.org/10.1021/jm501562a.
Scheers, E., Borgmans, C., Keung, C., Bohets, H., Wynant, I., Poggesi, I., Cuyckens, F., Leclercq, L., Mamidi, R.N.V.S., 2021. Metabolism and disposition in rats, dogs, and humans of erdafitinib, an orally administered potent pan-fibroblast growth factor receptor (FGFR) tyrosine kinase inhibitor. Xenobiotica 51, 177–193. https://doi.org/10.1080/00498254.2020.1821123.
Schmid, U., Liesenfeld, K.-H., Fleury, A., Dallinger, C., Freiwald, M., 2018. Population pharmacokinetics of nintedanib, an inhibitor of tyrosine kinases, in patients with non-small cell lung cancer or idiopathic pulmonary fibrosis. Cancer Chemother. Pharmacol. 81, 89–101. https://doi.org/10.1007%2Fs00280-017-3452-0.
Smith, S.A., Waters, N.J., 2019. Pharmacokinetic and pharmacodynamic considerations for drugs binding to alpha-1-acid glycoprotein. Pharm. Res. 36, 30. https://doi.org/10.1007/s11095-018-2551-x.
Sudlow, G., Birkett, D.J., Wade, D.N., 1975. The characterization of two specific drug binding sites on human serum albumin. Mol. Pharm. 11 (6), 824–832.
Summerfield, S.G., Yates, J.W.T., Fairman, D.A., 2022. Free drug theory - no longer just a hypothesis? Pharm. Res. 39, 213–222. https://doi.org/10.1007/s11095-022-03172-7.
Tabernero, J., Infante, J.R., Mita, A., Keung, C., Skee, D., Xie, H., Parekh, T., De Porre, P., Luo, F.R., Soria, J.-C., 2016. Pharmacokinetics (PK) of the pan-FGFR inhibitor erdafitinib in urothelial carcinoma. Annals Oncol. Suppl. 6, 27. https://doi.org/10.1093/annonc/mdw373.17 vi266–vi295.
Tayyab, S., Sam, S.E., Kabir, Md.Z., Ridzwan, N.F.W., Mohamad, S.B., 2019. Molecular interaction study of an anticancer drug, ponatinib with human serum albumin using spectroscopic and molecular docking methods. Spectrochim. Acta A 214, 199–206. https://doi.org/10.1016/j.saa.2019.02.028.
US Food and Drug Administration. 2012 Iclusig® Product monograph https://www.accessdata.fda.gov/drugsatfda_docs/label/2012/203469lbl.pdf (accessed 18 July 2023).
Valeur, B., 2001. Molecular Fluorescence Principles and Applications. Wiley-VCH, Weinheim.
Wasan, K.M., Cassidy, S.M., 1998. Role of plasma lipoproteins in modifying the biological activity of hydrophobic drugs. J. Pharm. Sci. 87, 411–424. https://doi.org/10.1021/js970407a.
Wind, S., Schmid, U., Freiwald, M., Marzin, K., Lotz, R. Ebner, T., Stopfer, P., Dallinger, C., 2019. Clinical Pharmacokinetics and pharmacodynamics of nintedanib. Clin. Pharmacokinet. 58, 1131–1147. https://doi.org/10.1007%2Fs40262-019-00766-0.
Zsila, F., Iwao, Y., 2007. The drug binding site of human alpha1-acid glycoprotein: insight from induced circular dichroism and electronic absorption spectra. Biochim. Biophys. Acta 1770, 797–809. https://doi.org/10.1016/j.bbagen.2007.01.009.
Zsila, F., 2013. Subdomain IB is the third major drug binding region of human serum albumin: toward the three-sites model. Mol. Pharm. 10, 1668–1682. https://doi.org/10.1021/mp400027q.